Mechatronics 22 (2012) 1067–1077

Contents lists available at SciVerse ScienceDirect

Mechatronics

journal homepage: www.elsevier.com/locate/mechatronics

Modeling, control, and analysis of a robotic assist device

K. Alex Shorter [a], Yifan Li [a], Timothy Bretl [b], Elizabeth T. Hsiao-Wecksler [a,*]

[a] Department of Mechanical Science & Engineering, University of Illinois at Urbana Champaign, Urbana, IL, USA
[b] Department of Aerospace Engineering, University of Illinois at Urbana Champaign, Urbana, IL, USA

ARTICLE INFO

Article history:
Received 12 July 2011
Accepted 8 September 2012
Available online 22 October 2012

Keywords:
Gait assistance
Pneumatics
Solenoid valve
Proportional valve
Control systems
Biomechanics

ABSTRACT

This paper presents a model-based approach to control design for an existing lower-limb robotic assist device, the portable powered ankle–foot orthosis (PPAFO). This approach seeks to address two key limitations of the PPAFO caused by the use of solenoid valves: slow system response and inefficient actuation during assistance. System limitations were addressed using a proportional valve coupled with a modified control approach. The two different system configurations were compared in simulation and on an experimental test fixture during motion and torque control tasks. Root mean square (RMS) trajectory tracking error was used to evaluate system performance, while system efficiency was assessed by measuring pneumatic fuel consumed during each task. The proportional valve system reduced RMS tracking error by as much as 91%, and increased efficiency by as much as 95% over the solenoid valve system.

1. Introduction

The creation of robotic systems capable of assisting impaired individuals regain functionality offers the potential to yield significant advancements to the field of orthotics and will lead to new clinical treatment strategies for recovery and rehabilitation. Effective control of these mechanized assist devices is key to fully realizing their potential for this challenging application. Proper control enables the device to meet the functional requirements of an impaired individual during a task such as walking. Additionally, the ability to provide proper functional assistance enhances a clinician's ability to effectively manage an individual's recovery with the robotic system. For a cyclic functional task like walking, the control problem can be divided into two main parts: (1) the detection of gait events that determine control objectives for the device, and (2) the implementation of a control algorithm to meet the desired functional objective. Implementation of an algorithm depends on both the system hardware as well as the control architecture.

In this work, a model-based approach was chosen to address limitations in a recently developed robotic assist device, the portable powered ankle–foot orthosis (PPAFO). This design approach was selected because it provides access to information that might be unavailable in a purely experimental evaluation of the system. System modeling enables the designer to quickly evaluate performance in a relatively accurate virtual environment, reducing effort for both system hardware selection and control design. Additionally, the virtual environment allows the designers to address issues critical to the performance of the system well before the device is used by a patient.

Ankle foot orthoses (AFOs) are external devices used to correct lower limb gait deficiencies. The ideal AFO should accommodate the many aspects of gait that can be affected by injury or pathology during variable walking conditions, while being compact and lightweight to minimize the energetic impact to the wearer [1]. Currently prescribed AFOs are generally passive, light-weight plastic or carbon fiber devices that prevent unwanted foot motion with mechanical constraints [2–6]. However, since passive AFOs cannot provide supplemental torque assistance these prescription devices lack the flexibility to adapt to varying walking conditions and have a limited ability to accommodate different impairments.

Powered orthoses address these limitations through the combined use of sensors, actuators, and computer control to provide torque assistance and motion control for lower limb joints [7–13]. A specific example of a powered AFO is the portable powered ankle–foot orthosis (PPAFO), Fig. 1 [14]. The original configuration of the PPAFO provides both motion control and external torque assistance at the ankle with a bang–bang, event-based control scheme and is capable of operation outside of the laboratory or clinic (Fig. 2). Events were defined by the configuration of the body during the gait cycle and were used to determine the timing of PPAFO control objectives during gait. These objectives were to prevent uncontrolled motion of the foot during loading response (foot slap), provide supplemental torque during stance to assist propulsion, and control the motion of the foot to maintain foot clearance during limb advancement. Objectives were based on the functional tasks required for gait [15–18].

* Corresponding author. Tel.: +1 217 333 3415.
E-mail address: ethw@illinois.edu (E.T. Hsiao-Wecksler).

0957-4158/$ - see front matter © 2012 Elsevier Ltd. All rights reserved.
http://dx.doi.org/10.1016/j.mechatronics.2012.09.002

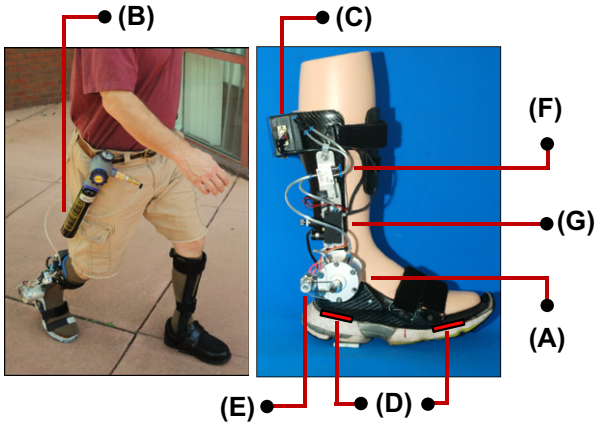

Fig. 1. The portable powered ankle–foot orthosis (PPAFO). The rotary actuator (A) is powered using a compressed CO_2 bottle (B) worn by the subject on the waist. Onboard electronics (C), force sensors (D), and an angle sensor (E) are used to control the solenoid valves (F). A second pressure regulator (G) is used to modulate the magnitude of the dorsiflexor assistance.

The ability of the PPAFO to provide functional assistance for individuals with both plantar and dorsiflexor deficits has been demonstrated experimentally [19], but the current system has several shortcomings. In particular, the current PPAFO design restricts the control objectives to those achievable with constant magnitude torque, and the bang-bang switching scheme utilized with the solenoid valves limits the efficiency of the system. This paper will address the current performance and efficiency limitations by replacing the solenoid valves with a proportional valve, and quantify performance improvements with a model-based system analysis. The proportional valve, along with the implementation of improved control design, will enable a variable torque output for motion control and propulsive assistance. These advancements allow this device to provide a wider range of functional assistance during gait. Performance and efficiency of the modified and original systems will be compared in both simulation and on an experimental test fixture during three trajectory tracking tasks that are simplified representations of functional requirements of walking gait. System performance will be evaluated on the accuracy of the task reference tracking, while system efficiency will be assessed by measuring pneumatic fuel consumed during each task. The results presented in this paper will demonstrate improvements to both performance and efficiency of the system during the tasks.

The contribution from this paper is twofold. First, this work provides an illustrative example of how to effectively utilize a well-identified system model to direct hardware design as well as develop and test different control strategies for a robotic assist device. Second, the model developed here can be used by other researchers working with pneumatic systems.

Specifically, this paper will begin with the derivation of a model of the current system, the combined system of the PPAFO with rigid-body human foot and shank segments with solenoid valves (Section 2). Section 2 will also introduce a second model incorporating a proportional valve for comparison with the current system. Parameters for the models will be identified using a system identification approach and will be followed by model validation. In Section 3, a strategy for evaluating the PPAFO hardware and control algorithms will be presented. The performance of the two PPAFO valve configurations will be examined during three tasks designed to emulate the functional requirements of a user during gait. Simulated and experimental results are used to demonstrate strengths and weaknesses of the different hardware configurations. Section 4 will provide a discussion of the results, followed by concluding remarks and future directions in Section 5.

2. Modeling, system identification, and model validation

2.1. PPAFO system hardware

The PPAFO is shown in Fig. 1 [14]. The system is pneumatically powered via a portable compressed liquid CO_2 bottle and pressure regulator (JacPac J-6901-91; Pipeline Inc., Waterloo, Canada) that can be worn at the waist. The pressure regulator at the bottle modulates the CO_2 supply pressure to the dual-vane bidirectional rotary actuator (CRB2BW40-90D-DIM00653; SMC Corp of America, Noblesville, IN, USA) at the ankle joint.

The torque generated by the actuator was used to provide both torque assistance and motion control of the foot during gait. The timing of the torque assistance was determined by gait events detected using the PPAFO sensors. Two force sensors, and an angle sensor (force sensor: 402, 0.5″ circle; Interlink Electronics Inc., Camarillo, CA, USA; angle senor: 53 Series; Honeywell, Golden Valley, MN, USA) provided the sensor feedback to identify gait events. During testing, two pressure transducers were used to measure actuator chamber pressure (4100 series; American Sensor Technology, Mt.Olive, NJ, USA). The data from PPAFO sensors and the additional pressure transducers were collected with a multifunction data acquisition (DAQ) module (NI-USB-6211, National Instruments and LabVIEW 2009).

2.1.1. Original hardware configuration: PPAFO with solenoid valves

The PPAFO in its original configuration [14] was operated with two solenoid valves (VOVG 5V; Festo Corp, Hauppauge, NY) as shown in Fig. 1. The solenoid valves are either fully open or closed and cannot be used to modulate actuator torque. Solenoid valves were initially selected for the PPAFO because of their small size, low power requirements, and low cost. One valve was used to pressurize the rotary actuator to generate dorsiflexor (toes-up) torque, and the other was used to generate plantarflexor (toes-down) torque. Because the magnitude of the dorsiflexor torque can be different than the plantarflexor torque required by an individual, an additional pressure regulator (LRMA-QS-4; Festo Corp. US, Hauppauge, NY) was used to modulate the dorsiflexor magnitude (Fig. 1).

While this configuration was successful at providing dorsi and plantarflexor torque assistance during gait, the hardware and control architecture have shortcomings. System performance was lim-

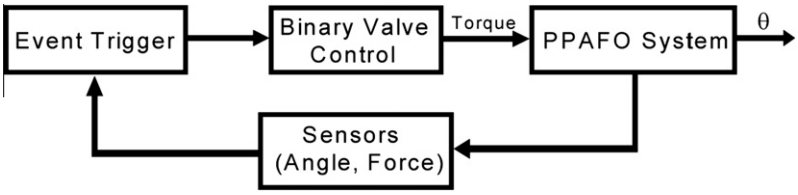

Fig. 2. Current binary control scheme used with the solenoid valves. PPAFO sensor data are used to identify the current gait event and open/close the corresponding valve.

ited by how the solenoid valves were used to provide functional assistance. Pressure regulators were first used to fix the magnitude of both the dorsiflexor and plantarflexor torque inputs. The solenoid valves were then used to control the timing of the assistance. As a result, the control scheme described in [14] was incapable of providing intermediate levels of torque assistance during gait. Additionally, the efficiency of the system was reduced by the high pneumatic power consumption that resulted from the all-on or all-off nature of the assistance.

2.1.2. Modified hardware configuration and control architecture: proportional valve

To address these issues the performance and efficiency limitations described in Section 2.1.1, a second PPAFO hardware configuration incorporating a single high-speed proportional valve (LS-V05s; Enfield Technologies, Trumbull, CT, USA) in place of the two solenoid valves was considered. A proportional valve enables variable levels of torque assistance, which allows for a wider range of potential control objectives.

In addition to a hardware change, a modified control architecture was implemented. Proportional valves are not restricted to the bang–bang control method utilized previously used with the solenoid valves. To improve the tracking performance and efficiency of the system, a proportional–integral–derivative (PID) control scheme was integrated into the system. A PID control scheme was initially selected based on its ease in implementation, prevalence in industry, and heuristic tuning methodology which enables online subject-specific tuning of the PPAFO if necessary. Performance results of the modified PPAFO are presented in Section 3.

2.2. Modeling of the PPAFO-Leg system

2.2.1. Modeling the PPAFO

Separate PPAFO system models including either solenoid or proportional valves were derived. To simplify the modeling, the solenoid valves were represented as fully open proportional valves with modified model parameters. The models consisted of the valve (solenoid or proportional), dual-vane rotary actuator, tubing between the valve and the actuator, and the added inertia of the actuator vane and PPAFO footplate (Fig. 3). The central vane is attached to the footplate, while the housing of the actuator is attached to the PPAFO structure on the shank. Pneumatic pressure differentials across the vane create rotational actuator torque. Hard stops prevent the vane from rotating more than 110°. The moment of inertia and damping of the vane of the rotary actuator and PPAFO footplate were modeled as a single rigid body because they are physically coupled at all times. The following assumptions were made:

(A1) constant pressure at the power supply;
(A2) no leakage within the system (except for leakage across the actuator vane);
(A3) homogeneous pressure inside each chamber;
(A4) negligible gas inertia;
(A5) isothermal processes in the chamber during expansion;
(A6) negligible line volume compared to the chamber;
(A7) negligible line loss between the power supply and actuator.

These assumptions were considered reasonable for the controlled experimental environment, the low working pressures, and the short activation times used during the experimental validation. Although some of these assumptions may need to be relaxed in an uncontrolled testing environment outside of a lab or clinic, they simplified the initial development of a model of the PPAFO-Leg system. Further analysis of these assumptions and their validity with respect to actual running conditions should be considered in future work.

The dynamics of the PPAFO were expressed as follows:

$$I_{zz}\ddot{\theta} + \beta\dot{\theta} + T_{gravity} + T_f + T_{ex} = T_{actuator}, \tag{1}$$

where θ is the angle of the vane (which also corresponds to the ankle joint angle of the coupled PPAFO-Leg system), I_{zz} is the moment of inertia of the footplate and actuator vane relative to the axis of rotation of the ankle joint, β is the rotary damping ratio, $T_{gravity}$ is the gravitational torque due to the weight of the PPAFO, T_{ex} represents the coupling torque between the PPAFO and the wearer (when modeling and identifying the PPAFO-Leg system it was set to zero), T_f is the friction torque opposing the motion of the vane, and $T_{actuator}$ is the output torque from the actuator (Fig. 3). Section 2.2.2 explains how model parameters were determined.

The actuator torque was approximated by the following equation [20],

$$T_{actuator} = (P_1 - P_2)K_{actuator}, \tag{2}$$

where $K_{actuator}$ is the experimentally determined torque-to-pressure ratio for the rotary actuator, and P_1 and P_2 are the pressures in the two actuator chambers, respectively. The instantaneous pressure in a given chamber was calculated using the ideal gas law,

$$P_i = \frac{m_i}{V_i M}RT, \quad \text{for} \quad i = 1, 2. \tag{3}$$

In Eq. (3), V_i is the volume of the actuator, m_i is the mass of CO_2 in the chamber and pneumatic lines, M is the molecular weight of CO_2 (44 g/mol), R is the universal gas constant (8.314 J/(K mol)), and T is the temperature of the gas (room temperature 298 K, constant due to isothermal assumption). The chamber volume can be expressed as a function of vane angle θ:

$$V_1 = B_{vane}\theta, \tag{4}$$

$$V_2 = B_{vane}(\pi/2 - \theta), \tag{5}$$

where B_{vane} is the volume-to-angle ratio for the rotary actuator.

The mass of CO_2 in each actuator chamber at a given time is calculated by integrating the mass flow rate $\dot{m}$ and is used to determine the pressures P_1 and P_2. The mass flow into and out of each actuator chamber was driven by pressure differentials within the system (P_{up} and P_{dn}) and was divided into two regimes (choked/non-choked) depending on the upstream and downstream pressures:

$$\text{choked flow}: \quad \frac{P_{up}}{P_{dn}} > \left(\frac{k+1}{2}\right)^{\frac{k}{k-1}} = 1.832,$$

$$\text{non-choked flow}: \quad \frac{P_{up}}{P_{dn}} < \left(\frac{k+1}{2}\right)^{\frac{k}{k-1}} = 1.832,$$

where $k = 1.3$ for CO_2, and P_{up} and P_{dn} are upstream and downstream pressure, respectively. Orifice plate flow theory was used to model the mass flow rate [21]. When the choked flow condition was satisfied, the mass flow rate was defined as,

$$\dot{m} = f(P_{up}, P_{dn}, A) = C_d A C_1 P_{up}, \tag{6}$$

where $C_1 = \sqrt{\frac{kM}{RT}\left(\frac{2}{k+1}\right)^{(k+1)/(k-1)}} = 0.00281$, C_d is the discharge coefficient, and A is the orifice cross-sectional area. When the non-choke condition was satisfied, mass flow rate was defined as

$$\dot{m} = f(P_{up}, P_{dn}, A) = C_d A C_2 P_{up}\left(\frac{P_{dn}}{P_{up}}\right)^{1/k}\sqrt{1 - \left(\frac{P_{dn}}{P_{up}}\right)^{(k-1)/k}}, \tag{7}$$

where $C_2 = \sqrt{\frac{2kM}{RT(k-1)}} = 0.0124$. The mass flow rate for our system, Eq. (7), was a function of upstream pressure P_{up}, downstream pressure P_{dn}, and the cross sectional area of the flow restriction [21,22].

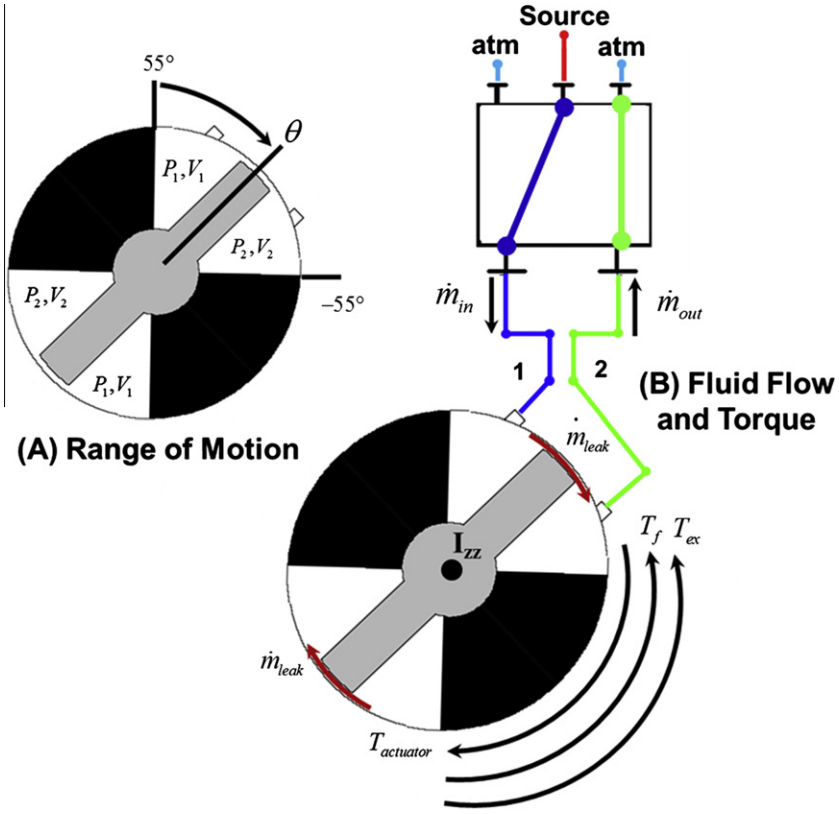

Fig. 3. The PPAFO pneumatic actuation system, shown with an idealized solenoid valve, consists of: a dual-vane rotary actuator, a solenoid or proportional valve, pneumatic lines, and the AFO footplate. Port 1 is connected to the source (regulated CO_2 bottle) and Port 2 is connected to atmosphere. Hard stops prevent the vane from rotating more than 110°. Leakage occurs between chambers ($\dot{m}_{leak}$). Additional symbols are defined in the text.

The coefficient A describes the equivalent orifice plate cross-section area and was the same for both Eqs. (6) and (7). The mass flow in the PPAFO came from three main sources: from the power source through the valve into one side of the actuator chamber $\dot{m}_{in}$, leakage from one chamber to another (across the actuator vane) $\dot{m}_{leak}$, and flow out of the actuator from the second chamber $\dot{m}_{out}$. Relationships for these mass flow rates are defined as:

$$\dot{m}_{out} = f(P_2, P_{atm}, A_{valve}), \tag{8a}$$

$$\dot{m}_{in} = f(P_{source}, P_1, A_{valve}), \tag{8b}$$

$$\dot{m}_{leak} = f(P_1, P_2, A_{leak}), \tag{8c}$$

$$\dot{m}_1 = \dot{m}_{in} - \dot{m}_{leak}, \tag{9a}$$

$$\dot{m}_2 = -\dot{m}_{out} + \dot{m}_{leak}, \tag{9b}$$

where P_{source} is the pressure at the supply (CO_2 bottle), A_{valve} is the cross-section area of the fully opened proportional valve orifice (a different A_{valve} was used for the solenoid valve), and A_{leak} is the equivalent cross-section area of the leakage pathway across the actuator vane.

Finally, the friction torque T_f from Eq. (1) can be expressed as,

$$T_f = \begin{Bmatrix} T_{f,static} & \text{if } \dot{\theta} = 0 \\ -sign(\dot{\theta}) \cdot T_{f,dynamic} & \dot{\theta} \neq 0 \end{Bmatrix}, \tag{10}$$

where $T_{f,static}$ is the static frictional torque. $T_{f,static}$ is equal and opposite the net actuator torque as long as its value falls below the experimentally determined maximum torque, $T_{static,max}$. Once the actuator torque exceeds $T_{static,max}$, the vane starts to move and the dynamic frictional torque, $T_{f,dynamic}$, begins to oppose vane motion. The sign of the dynamic frictional torque, $sign(\dot{\theta})$, is determined according to the actuator direction of rotation.

2.2.2. Identification of PPAFO model parameters

Several model parameters in the above equations were identified from indirect and direct experimental measurements, 3D modeling software, and component data sheets. The actuator torque-to-pressure constant ($K_{actuator}$), the static and dynamic frictional torques of the actuator ($T_{static,max}$ and $T_{f,dynamic}$), and rotary damping ratio (β) were determined experimentally. To identify the parameter $K_{actuator}$, static force measurements were made using a digital scale (Berkley, IA, USA) over a 95 psig (0.655 MPa) range. Three repetitions of measurements were made at increasing and decreasing 5 psig increments (0.034 MPa), Fig. 4 left panel. The average of the three sets of measurements was used to determine $K_{actuator}$.

The difference between the upward and downward measurements was a result of static friction. As pressure increased (denoted with an 'X'), static friction opposed vane motion reducing force measurements at the scale. The opposite effect occurred as pressure was decreased from 95 psig (denoted with an 'O') to 0 psig resulting in higher force measurements. The torque difference between data points at an equivalent pressure was twice the static frictional torque of the actuator ($T_{static,max}$ = 0.45 Nm). The resulting nominal pressure torque (bold line) lies between the data points. The slope of this line was defined as the actuator torque-to-pressure constant ($K_{actuator} = 1.451 \times 10^{-5} m^3$).

The PPAFO rotary damping ratio (β) was determined through a multi-step process. First, the system was positioned horizontally

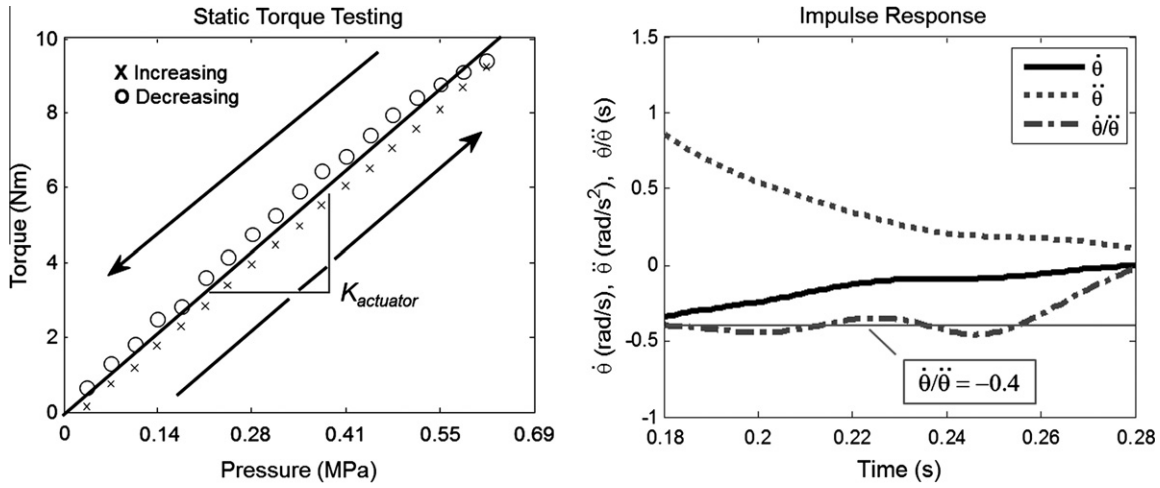

Fig. 4. Left panel: experimental determination of $K_{actuator}$. Measurements were taken as the pressure was increased by 5 psig (0.034 MPa) increments (denoted as X) to 90 psig (0.621 MPa) and then decreased by 5 psig increments back to 0 psig (denoted as O). Right panel: experimental determination of rotary damping ratio β. The ratio between the angular acceleration and the angular velocity is proportional to β, i.e., $\ddot{\theta}/\dot{\theta} = -\beta/I_{zz}$.

(with the ankle axis aligned with gravity) to minimize the impact of gravity. The parameters T_f, T_{ex}, and $T_{actuator}$ were all assumed to be equal to zero, which simplified the dynamics to,

$$I_{zz}\ddot{\theta} + \beta\dot{\theta} = 0. \tag{11}$$

Next, an impulsive force was applied to the end of the footplate. The resulting angular motion was recorded using the AFO angle sensor and used to calculate the corresponding angular velocity and acceleration. The damping ratio, $\beta = 0.02$ kg m^2/s, was approximated using the experimental data and the following equation:

$$\beta = -I_{zz} \cdot \frac{\ddot{\theta}}{\dot{\theta}}, \tag{12}$$

where the moment of inertia, $I_{zz} = 0.0084$ kg m^2, of the rotating components of the PPAFO system was calculated using 3D model software (Autodesk Inventor 2010, Autodesk, Inc. San Rafael, CA). The ratio, $\ddot{\theta}/\dot{\theta} = -\frac{1}{0.4}$, was determined from the experimental data at the end of the impulse response (Fig. 4 right panel). Data from the beginning of the trial were used to calculate the ratio $\ddot{\theta}/\dot{\theta}$ because the assumptions used to simplify the modeled system dynamics are valid in this region. Losses due to dynamic friction at velocities close to zero were then found using, $T_{f,dynamic} = -I_{zz}\alpha$, with $\alpha = 0.13$ rad/s^2 ($T_{f,dynamic} = 0.011$ Nm) also calculated from the experimental data.

Direct measurement of the fully open flow rate ($\dot{m}_{in} = 1.5$ g/s at 50 psig) through the valves was used to determine the parameters related to mass flow ($A_{valve} = 12.6$ mm^2 for the solenoid valve, $A_{valve} = 31.6$ mm^2 for the proportional valve, $C_d = 0.113$ s/m) used in Eqs. (9a) and (10). The parameter $A_{leak} = 0.3$ mm^2 in Eq. (8c) was identified by directly measuring the mass flow rate across the vane. The mass flow rate of the leakage across the actuator vane was measured to be $\dot{m}_{leak} = 0.045$ g/s at 50 psig. Finally, the volume to angle ratio of the actuator vane ($B_{vane} = 51$ cm^3/rad) was taken from the actuator data sheet.

2.2.3. Simplified model of the leg

A simple planar two-link rigid body model was used to represent the shank and foot segment of the leg (Fig. 5). The motion of the model was confined to the sagittal plane, and two degrees-of-freedom were used to define allowable configurations: the segment angle of the shank (φ), and the ankle joint angle (θ). Note that θ describes the motion of both the PPAFO vane and the ankle joint angle.

The dynamics of the leg model were derived using the Euler–Lagrange formulation,

$$\mathbf{M}(\mathbf{q})\ddot{\mathbf{q}} + \mathbf{C}(\dot{\mathbf{q}},\mathbf{q})\dot{\mathbf{q}} + \mathbf{G}(\mathbf{q}) = \begin{Bmatrix} T_1 \\ T_2 + T_{ex} \end{Bmatrix}, \tag{13}$$

$$\text{where, } \mathbf{q} = \begin{Bmatrix} \phi \\ \theta \end{Bmatrix}. \tag{14}$$

In Eq. (13), $\mathbf{M}(\mathbf{q})$ is the inertia matrix, $\mathbf{C}(\dot{\mathbf{q}},\mathbf{q})$ is the damping matrix and contains the centrifugal and Coriolis terms, $\mathbf{G}(\mathbf{q})$ is the gravity vector, T_1 is the subject-generated knee joint torque, T_2 is the subject-generated ankle joint torque, and T_{ex} is the torque applied to the leg model from the PPAFO, also defined as the coupling torque in Eq. (1) [23]. The physical parameters of the model are based on anthropometric measurements from a young adult male: $l_{shank} = 0.46$ m, $l_{foot} = 0.18$ m, $m_{shank} = 4.5$ kg, $m_{foot} = 1.0$ kg, $I_{zzshank} = 0.1$ kg m^2 and $I_{zzfoot} = 0.001$ kg m^2. Experimental kinematic walking data without the PPAFO from the same individual were used to calculate the shank segment states, $\phi and \dot{\phi}$. Because the motion of the shank is prescribed, the knee joint torque (T_1) is also determined by the experimental data. The experimental protocol was approved by the institutional review board and informed consent was obtained. Additionally, to further simplify the model, the ankle joint torque of the model was assumed to be zero ($T_2 = 0$), simulating a 100% neuromuscular deficit. This assumption was reasonable because a low friction mechanical joint approximated the ankle joint on the test

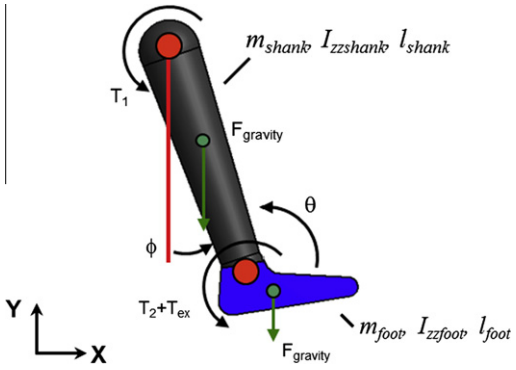

Fig. 5. The two-link rigid body leg model is coupled to the PPAFO through the applied external torque T_{ex}. Additional symbols are defined in the text.

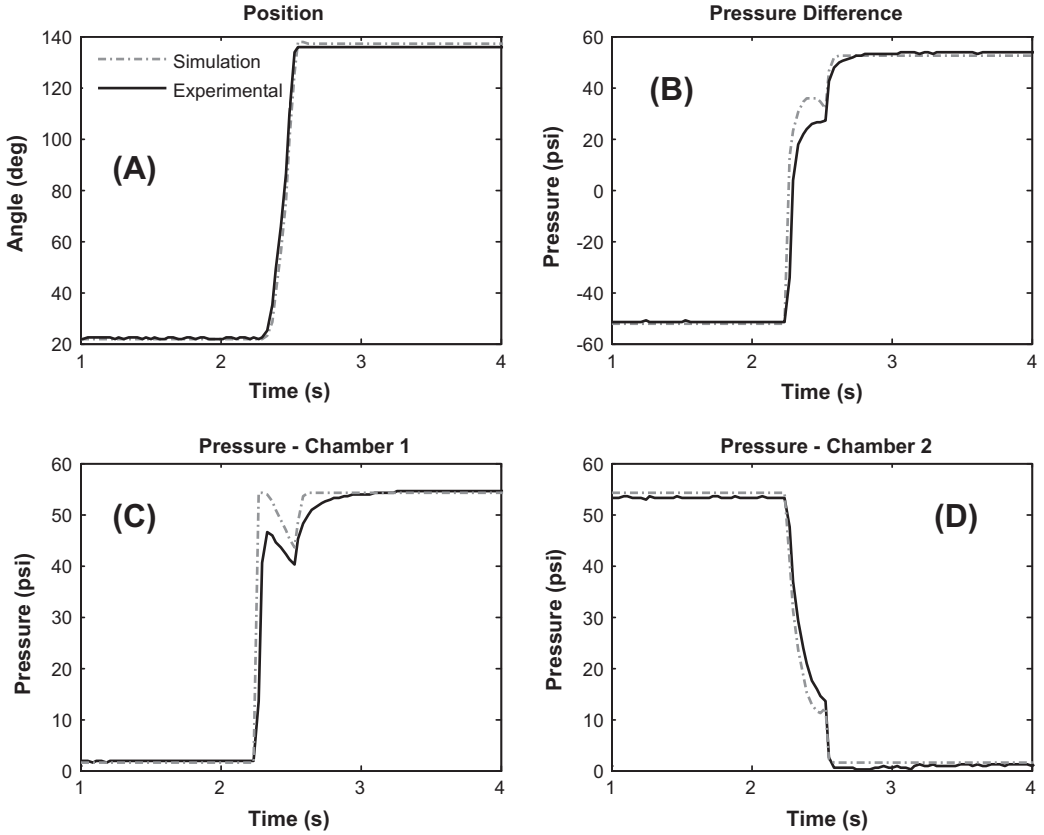

Fig. 6. Simulated and experimental open-loop coupled PPAFO-Leg system response to a step function with the proportional valve in the dorsiflexor direction. (A) The vane angle increased through the actuator's full range of motion (110°); (B) the pressure differential driving the actuator; (C) the pressure response in the first chamber (P_1); (D) the pressure (P_2) in the second chamber fell as the vane rotated. Experimental and simulated results compare well.

fixture used during experimental testing (Fig. 4B). The nominal impedance of the tendons and soft tissue of the ankle joint should be considered in future work. The PPAFO was used to control the motion of the model foot through the applied torque Tex. Eqs. (1) and (13) were then used to calculate θ. Simulations were built and run in the MATLAB Simulink (MathWorks, Natick Massachusetts, USA) environment.

2.3. PPAFO-Leg model validation

A step response was used to experimentally validate the coupled open-loop models of the system. The source pressure was set to 55 psig, and the PPAFO moved across the entire range of motion. Experimental joint angle data and pressure data from the two external transducers were collected to validate the simulation results. A step response was selected because it is typical of the simplified functional tasks that were used to evaluate system performance in Section 3.3. Only the model that incorporates the proportional valve was presented in this section because the solenoid valve is essentially the same system with a different orifice cross-sectional area.

During the experimental validation of the model, similar trends between simulation and experiment were observed in the position and pressure response. The displacement of the vane, pressure in both chambers and the pressure difference across the vane are shown in Fig. 6. As can be seen from the figure, the pressure initially increased inside Chamber 1 until the vane's maximum static friction ($T_{static,\max}$) was exceeded and the vane began to move (Fig. 6A). At this point, the pressure in Chamber 1 decreased as the volume, V_1, was increased by the moving vane. This lasted until the vane rotated to the other side of the actuator and stopped. After the vane ceased moving, the pressure in Chamber 1 increased to the source pressure and stabilized (Fig. 6C). On the other hand, the pressure in Chamber 2 (Fig. 6D) began at the source pressure and fell when the valve was opened. As the vane moved, the rate at which the pressure was dropping briefly slowed. This rate reduction was due to the compression of the CO_2 in Chamber 2, which occurred briefly before equalizing to atmospheric pressure.

The agreement between model-predicted and experimental results for the PPAFO are of particular note because they illustrate the fidelity of the model. During the step response, the root mean square (RMS) errors between the simulation and the experimental results for the vane position and pressure were within an acceptable range (10% of the full range): vane position (2.1°, 1.9% of the full range: 110°), pressure in chamber 1 (3.7 psi, 6.8% of the full range: 55 psi), pressure in chamber 2 (1.4 psi, 2.6% of the full range: 55 psi) and pressure difference (4.8 psi, 4.4% of the full range: 110 psi). Differences between predicted and experimental response of the pressure are due to the potential presence of unmodeled system dynamics, such as higher-order dynamics and resonances that were not captured by the simplified model. Additionally, taking changes in CO_2 temperature into account could also improve model accuracy.

3. Model-based system analysis and control design

The models derived and validated in Section 2 were then used to evaluate the new hardware configuration and control scheme (Fig 7) that seek to address performance and efficiency limitations of the solenoid valves used in the current PPAFO system. Three

simplified tasks that emulate ankle function during gait were selected to evaluate the performance and efficiency of the different system configurations.

3.1. Description of functional tasks required for gait

3.1.1. Ankle function during gait

Walking consists of cyclic motion patterns that are divided into gait cycles beginning and ending at consecutive ground contacts (heel strikes) of the same limb, and are typically on the order 1 Hz. Each cycle can be further subdivided into phases corresponding to the functional tasks required for gait [15]. The ankle joint plays an important role in these functional tasks. At the initiation of the gait cycle, during loading response, the muscles that power the ankle are used to decelerate the foot to foot flat preventing foot slap [2]. During mid and terminal stance, plantarflexor torque generated at the ankle is used for forward propulsion [16,17]. Finally, during swing, dorsiflexor muscles of the ankle joint are used to control the motion of the foot to maintain toe clearance, preventing foot drop, as the swing leg is advanced [15]. Lower limb pathology or injury that impairs dorsi and/or plantarflexor muscles has the potential to disrupt some or all of these functional tasks. In the next section, the role of the ankle joint was simplified to three key functional tasks that were used to define the control objectives for the PPAFO and assess system performance.

3.1.2. Simplified functional tasks used for system comparisons

Three control objectives were defined for the PPAFO system: (1) motion control of the foot at heel strike to prevent foot slap, (2) torque control during stance to aid propulsion, and (3) position control during swing to prevent foot drop (Fig. 8A–C). Experimental testing of the PPAFO was performed on a test fixture consisting of a rigid aluminum stand, and a mock leg and shank with rotational freedom at the ankle and knee joints (Fig. 9). The inertial properties of the mock leg matched the parameters used with the simplified leg model presented in Section 2. A test fixture was used because it provided a more controlled environment for the system evaluation than a human subject.

In Task 1, the PPAFO was used to control the motion of the foot at initial contact (Fig. 8A). Following ground contact at heel strike, the foot continues to rotate around the ankle joint until it is flat on the ground. Joint impairment can lead to an uncontrolled motion that results in an audible slap when the forefoot contacts the ground (foot slap). During this task, the control objective was to track an angular position reference trajectory designed to bring the foot to the ground at a constant velocity. For simplification, the shank angle was assumed to be held at a constant angle.

In Task 2, the PPAFO provided assistive plantarflexor torque for propulsion assistance during stance (Fig. 8B). In this task, the PPAFO was used to track a torque profile consisting of a ramp and a step function. This simplified profile emulated the behavioral trend seen in torque profiles from healthy walkers. For simplification, the entire foot segment remained in contact with the ground for the duration of the task, and the test fixture shank motion was generated manually.

The objective of Task 3 was to prevent the foot from dropping below neutral (90°) during swing (Fig. 8C). The foot was initially

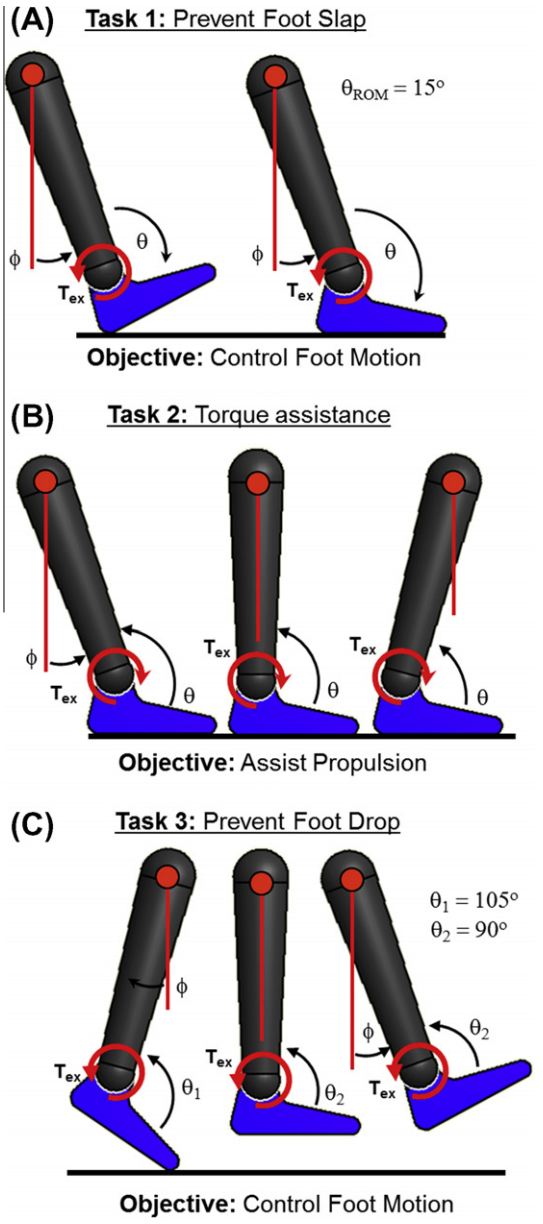

Fig. 8. The coupled PPAFO-Leg model shown during three functional tasks: (A) prevention of foot slap, (B) propulsive torque assistance, and (C) prevention of foot drop.

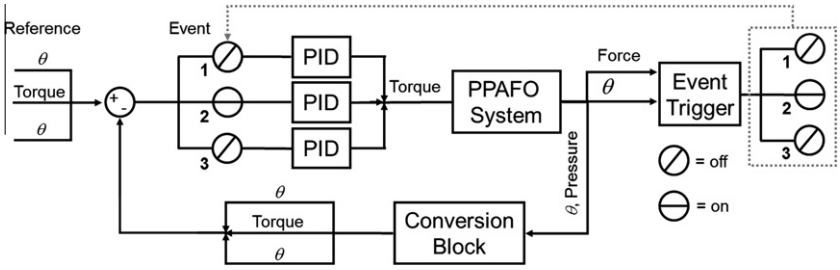

Fig. 7. Proposed control architecture that makes use of separate PID controllers to accomplish three functional gait tasks by tracking different variables.

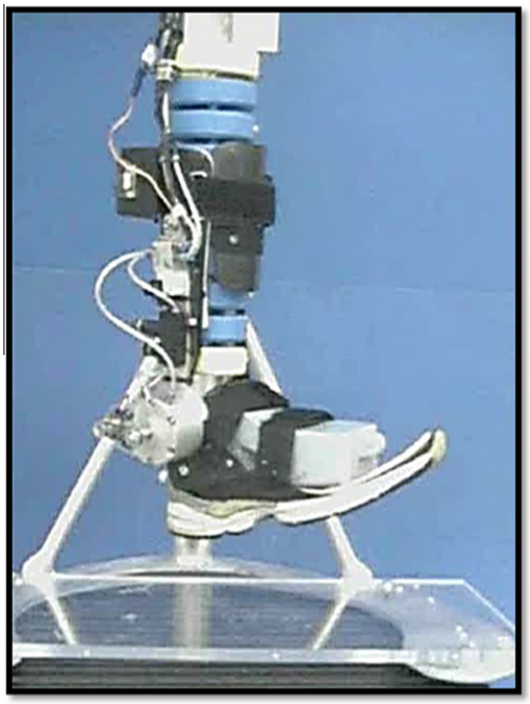

Fig. 9. The PPAFO shown on an experimental test fixture consisting of a rigid aluminum stand, and a mock foot and shank with rotational freedom at the ankle and knee joints.

plantarflexed 30° to correspond to an approximate configuration of the foot at the stance–swing transition. Next, the PPAFO was used to hold the foot at its neutral 90° position in order to prevent foot drop.

3.2. PPAFO control design

Having identified three key functional tasks, a control approach capable of achieving these tasks was designed. For simplicity and ease of implementation, PID controllers were used to control the proportional valve. The controllers had the form,

$$U_{\mathrm{Pro}} = k_p + k_i \frac{1}{s} + k_d s, \tag{15}$$

where k_p is the proportional gain, k_i is the integral gain, and k_d is the derivative gain. These gains were determined through heuristic tuning for each task. The control objectives in Task 1 included controlling the motion of the foot at initial contact, minimizing the tracking error between the PPAFO angle and the reference angle, and designing the system to meet specific performance requirements in terms of response time and overshoot of the PPAFO angle. In Task 2, the control objectives consisted of generating plantarflexor torque for propulsion assistance during stance and minimizing the root mean square (RMS) tracking error between the PPAFO torque and a desired reference torque. Lastly, the control objectives for Task 3 involved controlling the position of the foot during swing, minimizing the tracking error between the PPAFO angle and the desired angle, and meeting specific design requirements such as response time and overshoot of the PPAFO angle. Values for these heuristically-determined PID controller gains are given in Table 1. The same gains were used to generate both simulated and experimental results.

The solenoid valves were controlled in a binary manner, where the input control voltage to the valves was driven by a digital on/off signal. Since the two solenoid valves were controlling opposite sides of the rotary actuator, the control signals were always out of phase. The control signals for the two solenoid valves (U_A and U_B) were generated by a simple rule: if the error e was greater or equal than zero, trigger only valve A (setting it to +5 V) otherwise trigger only valve B. A dead-zone was not implemented with this system because the slow switching time of the valves created a large delay that would have been amplified by an additional dead-zone.

$$U_{sol} = \begin{cases} e \geqslant 0 & U_A = +5 \\ & U_B = 0 \\ e < 0 & U_A = 0 \\ & U_B = +5 \end{cases}. \tag{16}$$

3.2.1. Performance parameters

To compare the two valve configurations, as well as the modified PID control architecture, the following system performance parameters were examined: root mean square (RMS) errors between the reference and system outputs for assistive torque, angular position, and angular velocity of the PPAFO; response time and overshoot of angular position; and CO_2 consumption. After tuning the controllers to maximize system performance during the functional tasks, the system that consumed the least stored energy (CO_2) was considered the more efficient system.

3.3. Experimental and simulation results

The RMS tracking errors from the experimental results illustrated that the proportional valve significantly outperformed the solenoid valves in all three tasks, Table 2. This was especially apparent during Tasks 1 and 3 where the RMS errors for the proportional valve were decreased 91% and 86% over the solenoid valve, respectively. Additionally, the experimental CO_2 consumption was sizably smaller, up to 91%, across the three tasks, Table 2. The solenoid valves consumed 9.6 g while the proportional valve consumed 0.8 g during the trials. The three tasks took a total of ~8 s to complete, but during the experimental analysis of the two system configurations, the functional tasks were performed separately.

3.3.1. Task 1: motion control of the foot to prevent foot-slap

The goal of Task 1 was to control the motion of the foot after heel contact. The solenoid valves showed poor performance throughout the task as illustrated by the 91% increase in experimental RMS error as compared to the proportional valve. The source of these errors can be seen in the top panel of Fig. 10 as oscillatory behavior, which was unable to track the reference trajectory. On the other hand, the use of the proportional valve resulted in improved tracking performance throughout the task (bottom panel of Fig. 10). An additional benefit of the proportional valve was the reduced CO_2 consumption. The proportional valve consumed approximately 95% less CO_2 than the solenoid valves.

While the use of a proportional valve significantly improved the system performance, there were a few disadvantages that should be discussed. Although the system did display a relatively slow setting time to steady-state, the main disadvantage of the proportional valve was the 0.2 s delay at the initiation of the ramp transition, Fig. 10 bottom panel. This delay could be due to either

Table 1
Proportional valve PID gains for the three task controllers.

	K_p	K_i	K_d
Task 1	0.045	0.05	0.0052
Task 2	0.095	0.25	0.006
Task 3	0.045	0.05	0.0052

Table 2
Performance of the proportional and solenoid valves during the three functional tasks.

Functional task	Valve type	RMS tracking error	CO_2 consumption (g)
Task 1	Solenoid	33.9 (°)	2.0
	Proportional	3.0 (°)	0.1
Task 2	Solenoid	16.0 (Nm)	1.1
	Proportional	13.7 (Nm)	0.4
Task 3	Solenoid	45.2 (°)	6.5
	Proportional	6.3 (°)	0.3

the slow sampling rate or a physical limitation of this particular valve. Further investigations must be conducted in order to determine the cause of this delay. It is worth noting that delays may also have been present in the response of the solenoid valves, but the oscillatory behavior of the system made this difficult to observe.

3.3.2. Task 2: torque assistance during stance

In Task 2, the PPAFO was used to provide an assistive plantarflexor torque for propulsion assistance during stance. Although the 15% improvement in RMS tracking error was a smaller performance gain than seen in Task 1, the proportional valve still outperformed the solenoid valve. Additionally, the oscillatory behavior displayed by the solenoid valves during the initial ramp portion of the trajectory illustrated poor system performance that would not be desirable during actual implementation with an impaired subject, Fig. 11 top panel. The experimental results also demonstrated that the proportional valves had lower CO_2 consumption (63% less) than the solenoid valve.

3.3.3. Task 3: motion control during swing to prevent foot-drop

The objective during Task 3 was to control the position of the foot to maintain toe clearance during swing. The proportional valve was able to track the reference trajectory reasonably well, while the solenoid valve once again displayed oscillatory behavior and failed to perform this task, Fig. 12. As with Tasks 1 and 2, the proportional valve tracked the reference better than the solenoid valves during the experimental trials with an 86% smaller RMS tracking error. Additionally, the proportional valve consumed 95% less CO_2 during this task. Although the proportional valve resulted in improved performance over the solenoid valves, it still displayed a 0.2 s delay, had an overshoot of 30°, and required several seconds to settle to steady-state (Fig. 12 bottom panel). Again, delays may have been present in the response of the solenoid valves, but the oscillatory behavior of the system made this difficult to observe.

4. Discussion

Efficient and effective control of a powered AFO is crucial to maximizing the assistive benefit that an impaired user receives from the device. This work has emphasized that models that accurately approximate the behavior of an AFO system are central to effective control design, and that these models also facilitate the analysis and design of system hardware. Additionally, we have presented a well-identified model of a pneumatic robotic assist device, and well defined control objectives that can be used to evaluate the performance of the system.

Accordingly, the PPAFO system model derived in this work was used to design new control architecture and to evaluate the performance of both the current and modified PPAFO hardware configurations. The implementation of a proportional valve and new control methodology with the modified PPAFO system addressed two critical limitations identified in the current system: (1) an inability to generate intermediate levels of torque for assistance and motion control, and (2) high pneumatic power consumption caused by inefficient actuation.

The simulated and experimental results demonstrated that limitations in the current hardware configuration prevented the system from meeting the control objectives of Task 1 and Task 3. Further, this configuration only marginally met the objectives defined for Task 2. The performance of the solenoid valves was severely limited by the component-driven 20 Hz switching frequency. The slow switching frequency introduced significant

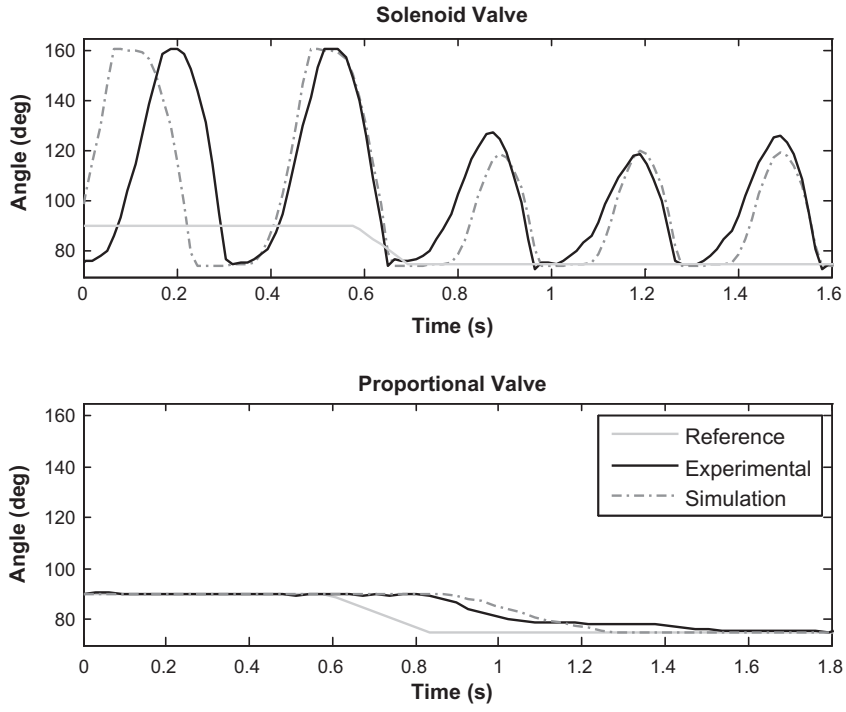

Fig. 10. Experimental and simulation results for motion control of the foot during functional Task 1: motion control of the foot during initial contact to prevent foot-slap.

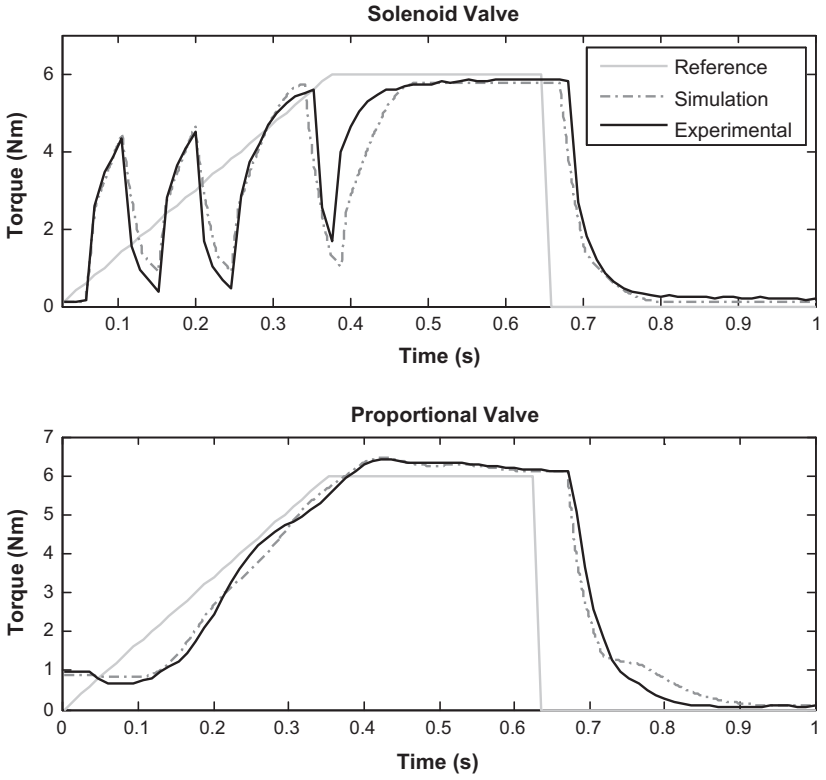

Fig. 11. Experimental and simulation results for the PPAFO with the solenoid valve (top panel) and the proportional valve (bottom panel) during Task 2: propulsive torque assist during stance.

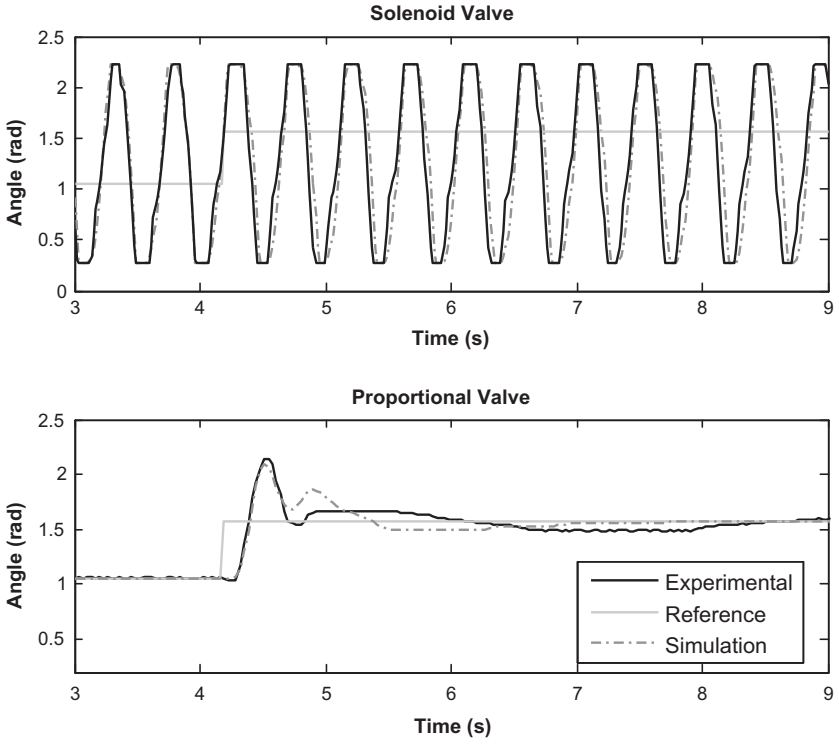

Fig. 12. Experimental and simulation results for the PPAFO with the solenoid valve (top panel) and the proportional valve (bottom panel) during Task 3: motion control of the foot during swing to prevent foot-drop.

delays that resulted in oscillatory behavior during the tasks, particularly those that required positional reference tracking. While these performance results clearly indicated the inability of the solenoid valves to switch fast enough for accurate torque or position tracking, this valve was originally selected due to its size and cost. Although the valve did show comparatively effective

assistance with respect to the original control objective of providing constant torque during the gait cycle, these additional results indicated the need for improved hardware.

The performance benefits from the proportional valve were apparent in the simulated and experimental results of Tasks 1 and 3. Unlike the solenoid valves, the proportional valve has the functional capability to modulate the system torque in order to track a changing reference. The use of the proportional valve with the system resulted in significant improvements in RMS tracking error over the solenoid valve, up to a 91% decrease. The proportional valve was also significantly more efficient, consuming 91% less CO_2 over the course of the three tasks. While the simulated and experimental results demonstrated that the proportional valve addressed the limitations in the current system, these results also highlighted certain areas for improvement in the modified design. Specifically, the delay in the actuation of the proportional valve is of particular concern, Figs. 10–12. Lengthy system delays could be particularly problematic for an assistive device because of the potential for an incorrectly timed control action that could disrupt gait. Additional disadvantages of proportional valves are the current size and weight of the valves and the control electronics, which do not make this valve very conducive to a compact portable device. Continued refinement of the systematic approach used to identify the PPAFO's torque requirements, and bumpless transfer techniques, similar to those presented in [13], would also benefit PPAFO control policy design. Future work will be directed towards addressing these limitations and performing an experimental evaluation of the modified system configuration with subjects during level walking.

5. Conclusion

Accurate models facilitate the design of control schemes that maximize the benefit a user derives from a robotic assist device. This work has resulted in a well-identified model of a pneumatic robotic assist device, the portable powered ankle–foot orthosis. This model was used to enhance the analysis of a new valving configuration and a new control scheme to address limitations in the current PPAFO system configuration. The results of this analysis demonstrated that the design changes to the PPAFO system presented here have the potential to significantly improve the performance and efficiency of the device. Additionally, the model developed in this work enables the continued improvement of hardware and control design, e.g. model based control algorithms. These improvements are crucial to transitioning the PPAFO system from a laboratory tool into a practical human assist device.

Acknowledgements

This work was supported by the NSF Engineering Research Center for Compact and Efficient Fluid Power grant #0540834, NSF CAREER grant #0955088, NSF grant #0931871 and NSF grant #0956362. The authors would like to thank Emily A. Morris and Aaron Becker for the contributions to this work.

References

[1] Waters RL, Mulroy S. The energy expenditure of normal and pathologic gait. Gait Posture 1999;9(July):207–31.
[2] Redford JB. Orthotics etcetera. Baltimore (MD): Williams and Wilkins; 1986.
[3] Rose GK. Orthotics: principles and practice. London: Williams Heinemann; 1986.
[4] Becker Orthopedic; 2003. <http://www.beckerorthopedic.com/cenfab/cfp.htm>.
[5] Kitaoka HB et al. The effect of custom-made braces for the ankle and hindfoot on ankle and foot kinematics and ground reaction forces. Arch Phys Med Rehabil 2006;87(January).
[6] Yamamoto S et al. Comparative study of mechanical characteristics of plastic AFOs. J Prosthet Orthot 1993;5(April).
[7] Furusho J, et al. Development of shear type compact MR brake for the intelligent ankle-foot orthosis and its control; research and development in NEDO for practical application of human support robot. In: IEEE 10th international conference on rehabilitation robotics, Noordwijk, The Netherlands; 2007. p. 89–94.
[8] Svensson W, Holmberg U. Ankle-foot-orthosis control in inclinations and stairs. In: IEEE international conference on robotics, automation and mechatronics, Chengdu, China; 2008. p. 301–6.
[9] Blaya JA, Herr H. Adaptive control of a variable-impedance ankle–foot orthosis to assist drop-foot gait. IEEE Trans Neural Syst Rehabil Eng 2004;12:24–31.
[10] Hwang S, et al. Development of an active ankle-foot orthosis for hemiplegic patients. In: Proceedings of the 1st international convention on rehabilitation engineering & assistive technology: in conjunction with 1st Tan Tock Seng Hospital Neurorehabilitation Meeting, Singapore; 2007.
[11] Hollander KW et al. An efficient robotic tendon for gait assistance. J Biomech Eng 2006;128(October):788–92.
[12] Hitt J, et al. Dynamically controlled ankle-foot orthosis (DCO) with regenerative kinetics: incrementally attaining user portability. In: 2007 IEEE international conference on robotics and automation; 2007. p. 1541–6.
[13] Yeh T-J et al. Control of McKibben pneumatic muscles for a power-assist, lower-limb orthosis. Mechatronics 2010;20(6):686–97.
[14] Shorter KA, Kogler GF, Loth E, Durfee WK, Hsiaoa-Wecksler ET. A portable powered ankle-foot orthosis for rehabilitation. J Rehabil Res Dev. 2011;48(4):459–72.
[15] Perry J. Gait analysis: normal and pathological function. Thorofare, NJ: Slack INC.; 1992.
[16] Neptune RR et al. Contributions of the individual ankle plantar flexors to support, forward progression and swing initiation during walking. J Biomech 2001;34(November):1387–98.
[17] Winter DA. Biomechanics and Motor Control of Human Movement. 3rd ed. Hoboken, New Jersey: John Wiley & Sons, INC.; 2005.
[18] Shorter KA, et al. Experimental evaluation of a portable powered ankle–foot orthosis. In: IEEE 33rd international conference of the engineering in medicine and biology society, Boston, USA; 2011. p. 624–7.
[19] Richer E, Hurmuzlu Y. A high performance pneumatic force actuator system: Part I—Nonlinear mathematical model. J Dyn Syst Meas Contr 2000;122:416–26.
[20] Munson BR et al. Fundamentals of fluid mechanics. New York: Wiley; 1990.
[21] Shen X et al. Nonlinear averaging applied to the control of pulse width modulated (PWM) pneumatic systems. J Dyn Syst Meas Contr 2006;128:7.
[22] Spong M et al. Robot modeling and control. John Wiley & Sons; 2006.
[23] Ren L et al. A phase-dependent hypothesis for locomotor functions of human foot complex. J Bionic Eng 2008;5(September):175–80.